AGU PUBLICATIONS

JGR

Journal of Geophysical Research: Oceans

RESEARCH ARTICLE

10.1002/2015JC010814

Ocean dynamical processes associated with the tropical Pacific cold tongue mode

Yang Li[1,2], Jianping Li[2,3], Wenjun Zhang[4], Xia Zhao[5], Fei Xie[2,3], and Fei Zheng[6]

[1]College of Atmospheric Science, Lanzhou University, Lanzhou, China, [2]College of Global Change and Earth System Science, Beijing Normal University, Beijing, China, [3]Joint Center for Global Change Studies, Beijing, China, [4]Collaborative Innovation Center on Forecast and Evaluation of Meteorological Disasters, Key Laboratory of Meteorological Disaster of Ministry of Education, Nanjing University of Information Science and Technology, Nanjing, China, [5]Laboratory of Ocean Circulation and Waves, Institute of Oceanology, Chinese Academy of Sciences, Qingdao, China, [6]State Key Laboratory of Numerical Modeling for Atmospheric Sciences and Geophysical Fluid Dynamics (LASG), Institute of Atmospheric Physics, Chinese Academy of Sciences, Beijing, China

Key Points:
- This study investigates the specific ocean dynamical processes related to CTM
- The four ocean advections exhibit a good relationship with CTM
- The advection by the mean upwelling dominates the long-term change of CTM

Supporting Information:
- Supporting Information S1

Correspondence to:
J. Li,
ljp@bnu.edu.cn

Citation:
Li, Y., J. Li, W. Zhang, X. Zhao, F. Xie, and F. Zheng (2015), Ocean dynamical processes associated with the tropical Pacific cold tongue mode, *J. Geophys. Res. Oceans*, *120*, 6419–6435, doi:10.1002/2015JC010814.

Received 6 MAR 2015
Accepted 19 AUG 2015
Accepted article online 25 AUG 2015
Published online 24 SEP 2015

Abstract The cold tongue mode (CTM) is the second EOF mode of sea surface temperature anomaly (SSTA) variability over the tropical Pacific and represents the out-of-phase relationship in SSTA variability between the Pacific cold tongue region and elsewhere in the tropical Pacific. A positive CTM is characterized by cold SSTA in the Pacific cold tongue region and warm SSTA in the rest of the tropical Pacific, with conditions reversed for a negative CTM. The CTM is a coupled air-sea mode, and its long-term variability is most probably induced by ocean dynamical processes in response to global warming [*Zhang et al*., 2010]. This study focuses on the specific ocean dynamical processes associated with the CTM and its possible relationship with global warming. A heat budget diagnosis of ocean temperature in the eastern equatorial Pacific shows that the net heat flux plays a damping role and the four ocean advection terms ($-u'\partial\bar{T}/\partial x$, $-\bar{v}\partial T'/\partial y$, $-\bar{w}\partial T'/\partial z$, and $-w'\partial\bar{T}/\partial z$) contribute to the temperature change associated with the CTM. Among them, the vertical advection of the anomalous temperature by the mean upwelling ($-\bar{w}\partial T'/\partial z$) makes a dominant contribution to the long-term change in the CTM. The long-term change of the term $-\bar{w}\partial T'/\partial z$ is controlled mainly by the decreasing vertical gradient of the ocean temperature anomaly ($\partial T'/\partial z$). The other three advection terms make a minor contribution to the long-term change in the CTM.

1. Introduction

The tropical Pacific drives the global climate by providing massive sensible and latent heat fluxes [*Cane*, 1998], and it has the most important natural climate mode at an interannual time scale (i.e., the El Niño/Southern Oscillation (ENSO) phenomenon) [e.g., *Rasmusson and Carpenter*, 1982; *Philander*, 1990; *Trenberth*, 1997]. ENSO has been the focus of much public concern because of its capacity to generate worldwide environmental and socioeconomic impacts [e.g., *McPhaden et al*., 2006]. Recently, a new flavor of ENSO, referred to as the Central-Pacific type (CP-ENSO), has been found to occur frequently in the tropical Pacific [*Ashok et al*., 2007; *Cai and Cowan*, 2009; *Kao and Yu*, 2009; *Kug et al*., 2009; *Yeh et al*., 2009; *Shinoda et al*., 2011; *Zhang et al*., 2014a]. Many studies have reported that its climatic impacts are remarkably different [e.g., *Weng et al*., 2007; *Cai and Cowan*, 2009; *Weng et al*., 2009; *Taschetto and England*, 2009; *Feng and Li*, 2011; *Zhang et al*., 2011, 2013a; *Wang and Wang*, 2013; *Zhang et al*., 2014a,b]. *Yeh et al*. [2009] argued that global warming is possibly responsible for the ENSO regime change. Generally, global warming affects ENSO characteristics by modifying the background of the tropical Pacific [e.g., *Fedorov and Philander*, 2000; *Yeh et al*., 2009; *Choi et al*., 2011; *Xiang et al*., 2013].

Large discrepancies remain among the various estimates of long-term change in the tropical Pacific under global warming [e.g., *Vecchi et al*., 2008; *Collins et al*., 2010]. *Meehl and Washington* [1996] suggested that cloud-albedo feedback triggers an El Niño-like pattern (i.e., greater warming in the east Pacific than in the west) as a result of reduced incoming solar radiation caused by a stronger cloud shielding effect in the west than in the east. This El Niño-like pattern has been identified in observations [*Graham*, 1995; *Wang*, 1995;

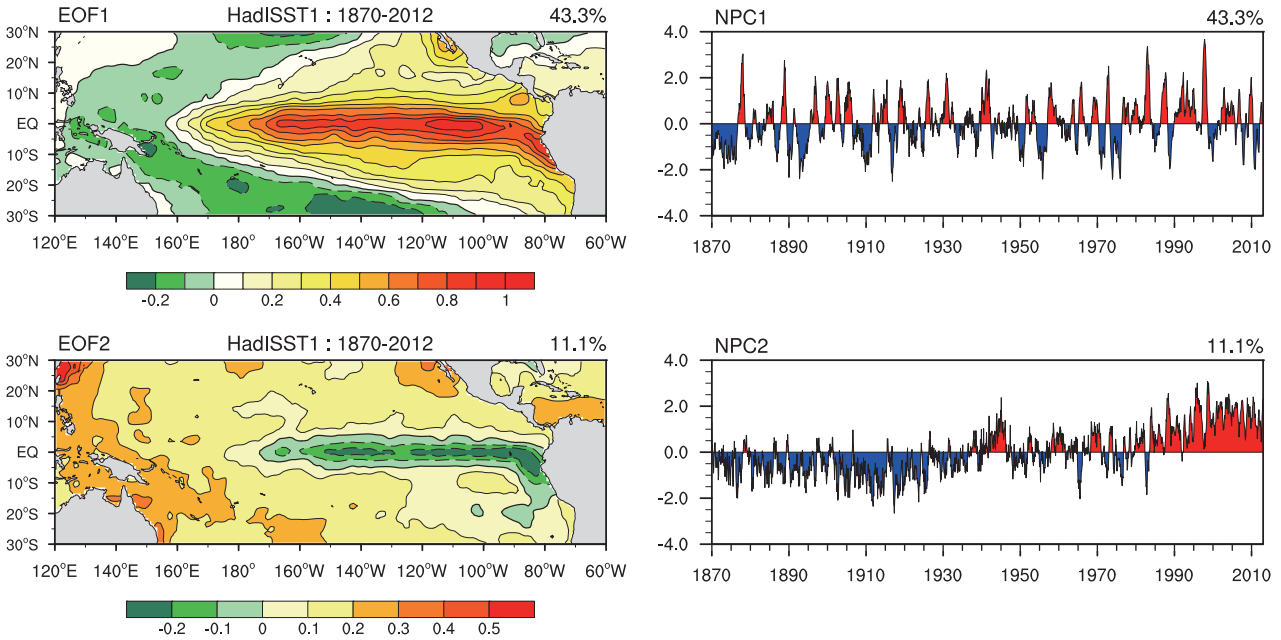

Figure 1. Spatial patterns and corresponding NPCs of the first two leading EOF modes of the tropical Pacific SSTA for the HadISST1 data set.

Trenberth and Hoar, 1996; *Zhang et al.*, 1997; *Knutson and Manabe*, 1998] and simulations [*Knutson and Manabe*, 1995; *Tett*, 1995; *Meehl and Washington*, 1996; *Roeckner et al.*, 1996; *Timmermann et al.*, 1999; *Cai and Whetton*, 2000; *Jin et al.*, 2001]. *Held and Soden* [2006] suggested that a decreasing zonal sea surface temperature (SST) gradient is also supported by a weakening atmospheric zonal overturning circulation as a response to global warming and argued that different increasing rates for water vapor and precipitation indicate a weakening mass exchange between the boundary layer and the free troposphere (i.e., a slowdown in atmosphere circulation). Therefore, the weakening Walker Circulation and thus the weakening trade winds cause the decreasing zonal SST gradient over the tropical Pacific [*Vecchi et al.*, 2006, *Vecchi and Soden*, 2007].

A La Niña-like pattern (i.e., greater warming in the west Pacific than in the east) has also been reported in observations [*Cane et al.*, 1997; *Karnauskas et al.*, 2009; *Compo and Sardeshmukh*, 2010; *Zhang et al.*, 2010; *Solomon and Newman*, 2012; *L'Heureux et al.*, 2013] and simulations [*Cane et al.*, 1997; *Noda et al.*, 1999; *Zhang et al.*, 2010]. An ocean dynamical feedback is suggested to be responsible for the La Niña-like pattern [*Clement et al.*, 1996; *Sun and Liu*, 1996; *Cane et al.*, 1997; *Seager and Murtugudde*, 1997; *Zhang et al.*, 2010], whereby vigorous upwelling of cold water in the eastern equatorial region causes the slower warming in the eastern Pacific than in the western Pacific. The mechanisms, which play a dominant role in long-term climate change over the equatorial Pacific, remain debated.

Compo and Sardeshmukh [2010] suggested that ENSO can be considered as a noise for the long-term change of global SST anomalies (SSTAs), and that it probably hinders our understanding of the long-term change in the tropical Pacific. Based on this assumption, some studies have analyzed the long-term change in the tropical Pacific SSTA and its associated Walker Circulation by removing the ENSO signal. *Solomon and Newman* [2012] demonstrated that the tropical Pacific SSTA long-term trend shows a La Niña-like pattern in four SST data sets (HadISST, ERSST, COBE, and Kaplan) when the ENSO signal is removed. This La Niña-like pattern is also found in 10 different sea level pressure (SLP) data sets after removing the ENSO signal [*L'Heureux et al.*, 2013]. These results suggest that the ocean dynamical feedback is a dominant influence on the long-term change over the tropical Pacific. To improve our understanding of the long-term variability in the tropical Pacific, it seems necessary to separate the ENSO signal from total variability. The residual variability may well reflect the relationship between long-term climate change in the tropical Pacific and global warming.

Previous studies have demonstrated that empirical orthogonal function (EOF) analysis can clearly identify the ENSO signal [*Rasmusson and Carpenter*, 1982; *Trenberth*, 1997; *Zhang et al.*, 2010]. Figure 1 shows the

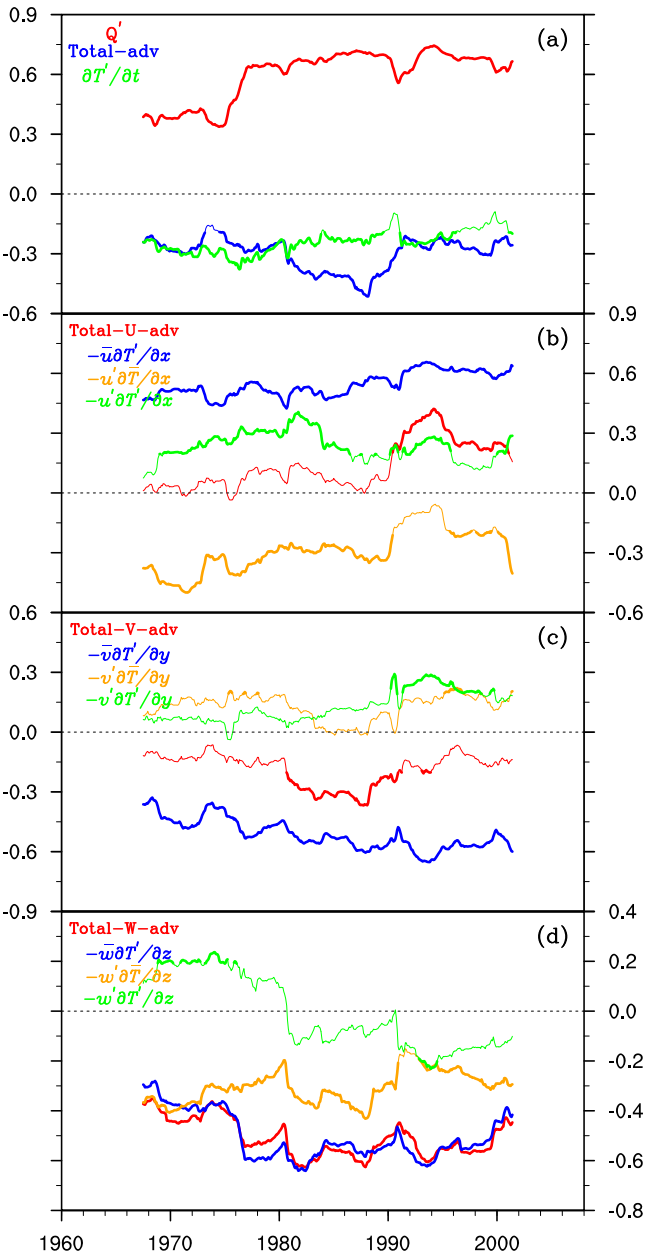

Figure 2. Time series of 15RCR between NPC2 and each advection term of the temperature equation in the eastern equatorial Pacific mixed layer (0–30 m, 2°S–2°N, 140°W–80°W). (a) Net heat flux (red line), total temperature advection (blue line), and temperature tendency (green line); (b) temperature advection by the zonal current; (c) temperature advection by the meridional current; and (d) temperature advection by the vertical current. In Figure 2b, red, blue, orange, and green lines indicate total zonal temperature advection, advection by the mean zonal current, advection by the anomalous zonal current, and the zonal nonlinear term, respectively. (Figures 2c and 2d) As in Figure 2b, but for the meridional and vertical temperature advections. Thicker lines indicate statistical significance at the 99% confidence level.

first two leading EOF modes over the tropical Pacific using the HadISST1 data set and their corresponding normalized principal components (NPCs). These modes account for 43.3% and 11.1% of the total variance, respectively. The first EOF mode mainly describes the ENSO variability, with the maximum SSTA in the eastern tropical Pacific. Its NPC1 is dominated by interannual variability. Aside from the ENSO mode, the second EOF mode depicts an out-of-phase relationship in SSTA variability between the Pacific cold tongue region and elsewhere in the tropical Pacific, referred to as a cooling mode (or cold tongue mode, hereafter CTM) [*Zhang et al.*, 2010]. The positive CTM is characterized by a cold SSTA in the Pacific cold tongue region and a warm SSTA in the rest of the tropical Pacific, and vice versa. Its NPC2 mainly exhibits a strong long-term variability in SSTA, with a negative phase before the late 1930s, oscillation during the period 1940–1980, and a positive phase after the early 1980s. *Zhang et al.* [2010] also stated that the CTM is a coupled phenomenon (in their Figure 5) and that its long-term variability is most probably induced by ocean dynamical processes in response to global warming. In addition, some studies have suggested that the La Niña-like background state in the tropical Pacific seems to cause the more frequent occurrence of the central Pacific (CP) El Niño in recent decades [*Choi et al.*, 2011; *Xiang et al.*, 2013]. *Duan et al.* [2014] used an optimal forcing vector (OFV) approach to offset tendency errors in a simulation of CP-El Niño in the Zebiak-Cane model [*Zebiak and Cane*, 1987]. They found that the offsetting pattern is similar to the CTM pattern. This means that the CTM may also have an effect on the ENSO regime change. As mentioned above, it is of great significance to study the CTM.

The above studies [e.g., *Cane et al.*, 1997; *Zhang et al.*, 2010; *Solomon and Newman*, 2012; *L'Heureux et al.*, 2013] suggested that the ocean dynamical feedback plays a dominant role in the long-term SST change over the tropical Pacific under global warming. However, the specific physical processes of ocean dynamical feedback under global warming are not clear. Consequently, we intend to address the following questions. Which ocean dynamical processes are primarily responsible for the ocean temperature change associated with the CTM? And, what are

the possible relationships between the ocean dynamical processes and global warming? The remainder of this paper is organized as follows. In section 2, we briefly introduce the observational data sets and methods. Section 3 analyzes the net heat flux and ocean dynamical processes associated with the CTM based on a heat budget for ocean temperature. Section 4 discusses the relationships between the ocean dynamical processes and global warming. Finally, conclusions and a discussion are presented in section 5.

2. Data and Methodology

2.1. Data

The SST data set used in this study was the Hadley Centre SST data set version 1 (HadISST1) on a 1° × 1° grid [*Rayner et al*., 2003]. We also used the fourth Met Office Hadley Centre and Climatic Research Unit Global Land and Sea Surface Temperature Data Set (HadCRUT4) on a 5° × 5° grid [*Morice et al*., 2012]. The ocean subsurface temperature, circulation, and sea surface wind stress data were from the Simple Ocean Data Assimilation (SODA 2.2.4) system [*Carton and Giese*, 2008]. This product has a 0.5° × 0.5° horizontal resolution with 40 vertical levels and covers the period 1871–2008. The data were produced by using an ocean general circulation model to assimilate available temperature and salinity observations. The surface boundary conditions of the ocean model were taken from the Twentieth Century Reanalysis version 2 (20CR2) [*Compo et al*., 2011]. The 20CR2 data set is a comprehensive global atmospheric circulation data set spanning the period 1871–2010 and contains a synoptic-observation-based estimate of global tropospheric variability. The 20CR2 reanalysis was also used to analyze the heat flux in the present study. However, the 20CR2 data set is probably unreliable during the first half of the twentieth century, because of the lower observational density in the earlier part of the record [*Compo et al*., 2011; *Krueger et al*., 2013]. Therefore, we used the period 1960–2008 for all data sets to analyze the ocean dynamical feedback associated with the CTM. The mean seasonal cycle of all data sets from 1961 to 1990 has been removed.

2.2. Methodology

Several statistical methods were used in this study. We used the normalized empirical orthogonal function (NEOF), in which the principal components were divided by their standard deviation (STD) and the spatial EOF patterns were multiplied by the corresponding STD [*Zheng et al*., 2013]. We also used the partial correlation, regression, and running correlation methods. The significance of the trends was tested using the nonparametric Mann-Kendall method. To determine the contributions of net heat flux and ocean advection terms to the CTM, the temperature heat budget was calculated. Following previous studies [e.g., *Kang et al*., 2001; *Kug et al*., 2009; *Ren and Jin*, 2013; *Zhang et al*., 2013b], the heat budget equation is shown as follows:

$$\frac{\partial T'}{\partial t} = -\bar{u}\frac{\partial T'}{\partial x} - u'\frac{\partial \bar{T}}{\partial x} - u'\frac{\partial T'}{\partial x} - \bar{v}\frac{\partial T'}{\partial y} - v'\frac{\partial \bar{T}}{\partial y} - v'\frac{\partial T'}{\partial y} - \bar{w}\frac{\partial T'}{\partial z} - w'\frac{\partial \bar{T}}{\partial z} - w'\frac{\partial T'}{\partial z} + Q' + R \tag{1}$$

where overbars and primes indicate the monthly climatology and anomaly, respectively. The variables u, v, w, T, Q', and R indicate zonal current, meridional current, vertical current, ocean temperature, thermal forcing, and residual terms, respectively. Note that R is not considered in this study and that Q' in the oceanic mixed layer can be determined from the expression:

$$Q' = \frac{Q'_{net}}{\rho C_p H} \tag{2}$$

where Q'_{net}, ρ, and C_p denote the net heat flux at the ocean surface, the density of water, and the specific heat of water, respectively. H is the climatological mixed layer depth, and $H = 30$ m in this paper.

3. Net Heat Flux and Ocean Dynamical Processes Associated With the CTM

3.1. Contribution of Net Heat Flux

As the time scale of the CTM is relatively long under global warming (Figure 1), we use the 15 year running correlation coefficient (15RCR) to diagnose the relationships between the CTM and temperature heat budget terms. Figure 2a shows the 15RCRs between NPC2 and the anomalous net heat flux, the anomalous total ocean advection, and the SSTA tendency in the eastern equatorial Pacific mixed layer (2°S–2°N,

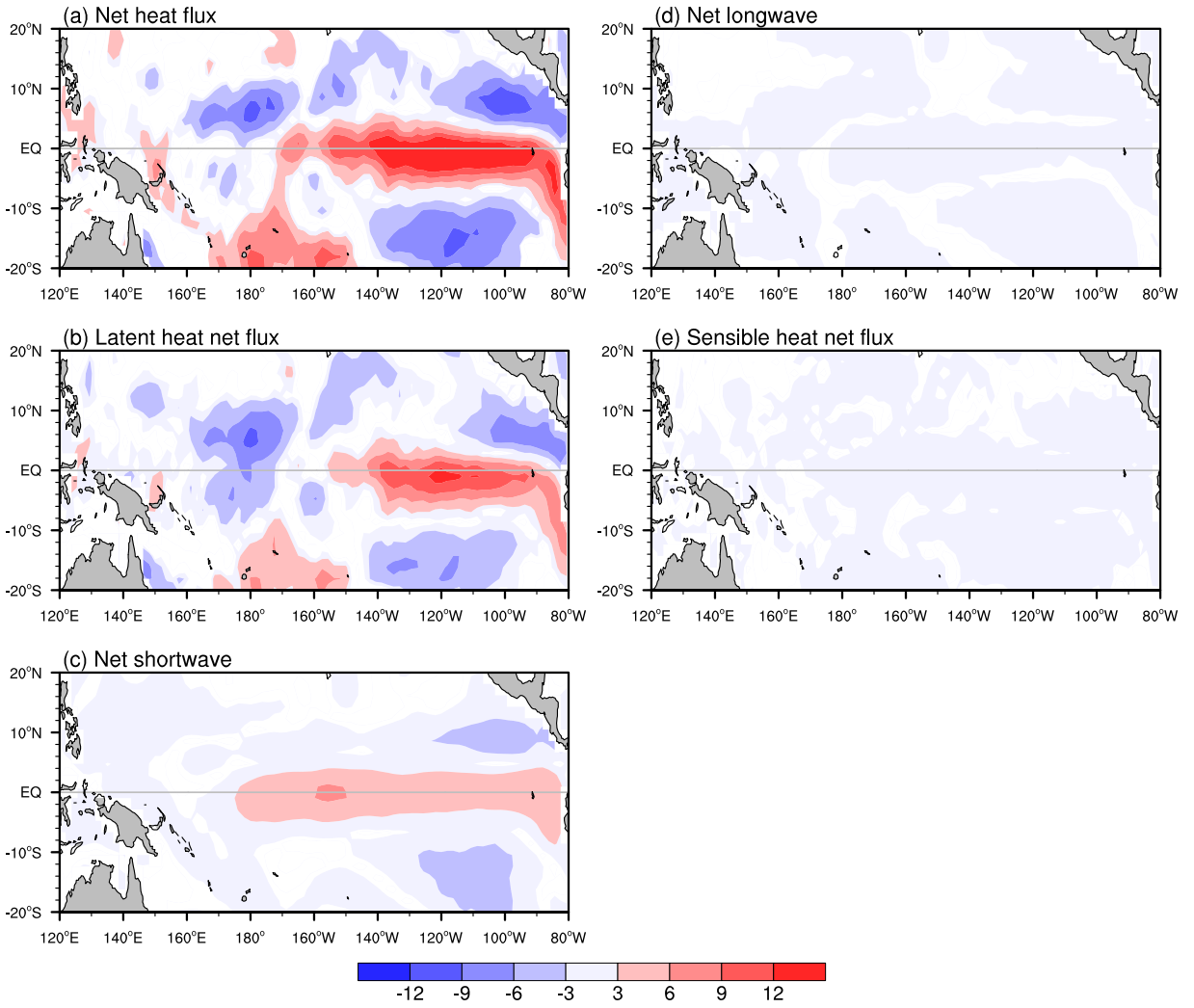

Figure 3. Regression of heat flux (positive downward; W m^{-2}) onto NPC2 over the period 1960–2008. (a–e) Net heat flux, latent heat net flux, net shortwave radiation flux, net longwave radiation flux, and sensible heat net flux, respectively. In all parts, shading indicates statistical significance at the 99% confidence level.

140°W–80°W). There is a stable positive 15RCR between NPC2 and the anomalous net heat flux. The positive CTM (cold SSTA in the cold tongue region) corresponds to positive net heat flux, and vice versa. We also show the anomalous net heat flux regressed onto NPC2 over the period 1960–2008 (Figure 3a). Positive anomalous net heat flux is located over the eastern equatorial Pacific and is associated with the cooling CTM. Furthermore, decomposition of the anomalous net heat flux into the anomalous latent heat net flux, net shortwave radiation flux, net longwave radiation flux, and sensible heat net flux indicates that the anomalous net heat flux associated with the CTM depends mainly on the anomalous latent heat net flux and the net shortwave radiation flux (Figure 3).

The effect of wind stress on the latent heat net flux is examined. Figure 4a shows the surface wind stress and divergence anomalies regressed upon NPC2 over the period 1960–2008. Divergence anomalies of surface wind stress occur over the eastern equatorial Pacific, where southwesterly and northwesterly wind stress anomalies prevail to the north and south of the equator, respectively. By averaging the regression coefficients between 2°S and 2°N, robust divergence anomalies appear east of the date line (Figure 4b). Strong easterly anomalies appear west of about 140°W (Figure 4b), and weak westerly anomalies occur east of about 140°W (Figures 4b and 4c). This result suggests that the local wind stress anomalies associated with the CTM over the eastern equatorial Pacific are opposite to the climate mean state of wind stress. This reduces the release of latent heat from ocean to atmosphere and consequently contributes to the positive net heat flux anomalies (Figure 3).

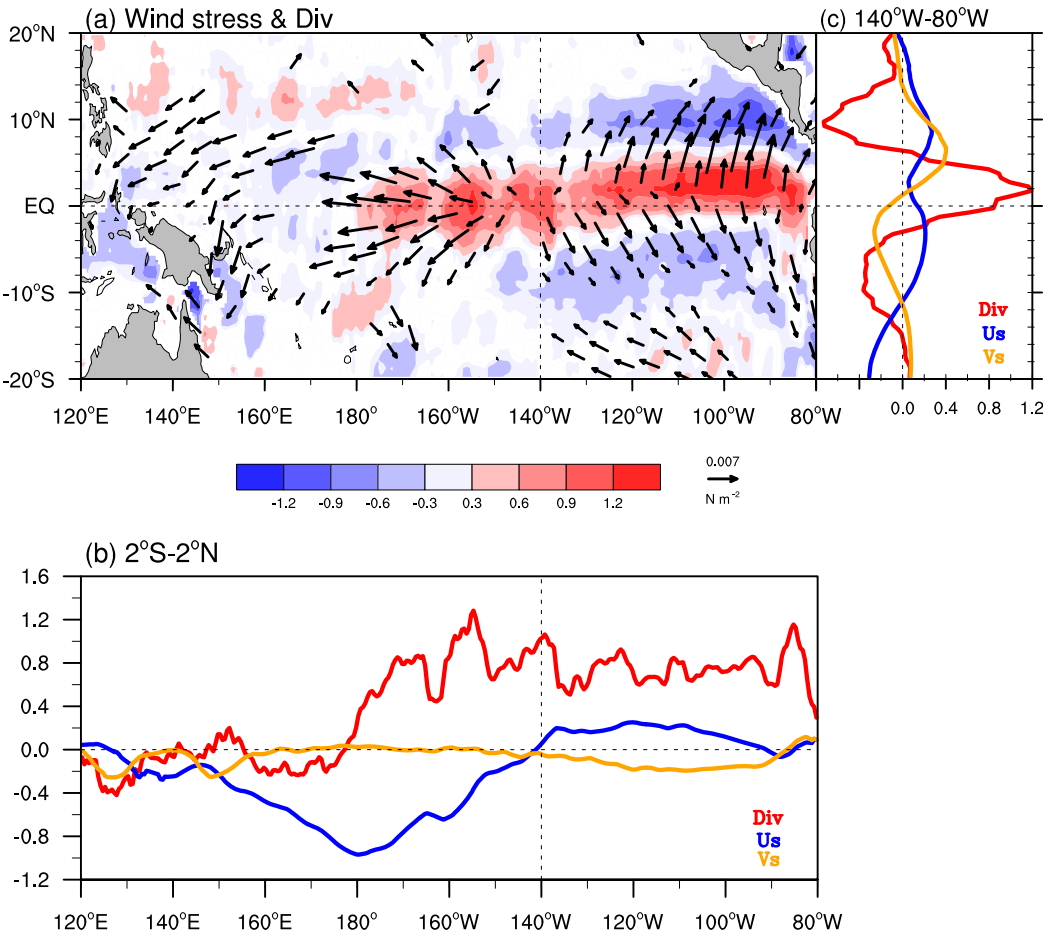

Figure 4. (a) Anomalies of surface wind stress (vectors) and its divergence (shading; 10^{-8} N m^{-3}) regressed on NPC2 over the period 1960–2008. Shading and black vectors indicate statistical significance at the 99% and 95% confidence levels, respectively. (b) Meridional average regression coefficients of Figure 4a from 2°S to 2°N for divergence (red line), zonal wind stress (blue line), and meridional wind stress (orange line). (c) As in Figure 4b, but for the zonal average from 140°W to 80°W.

The net shortwave radiation flux is related to the total cloud cover. In association with the positive CTM, anomalous atmospheric sinking appears over the central and eastern equatorial Pacific [*Zhang et al.*, 2010]. The sinking center is located over the central equatorial Pacific and can reach 150 hPa (Figure 5a). This anomalous sinking circulation could suppress the growth of cloud, resulting in a weaker cloud shielding effect in the eastern equatorial Pacific (Figure 5b). This means that the ocean is able to absorb a greater net shortwave radiation flux and thereby contribute to the positive net heat flux anomalies in this area (Figure 3).

3.2. Contribution of Ocean Advections

The above results suggest that the anomalous net heat flux acts as a damping term for the CTM. That is, the CTM-associated ocean temperature change should be closely related to the ocean dynamical processes (Figure 2a, blue line). To develop a better understanding of the role of each ocean advection term, we investigate their relationships with the CTM. Based on equation (1), the anomalous total ocean advection can be decomposed into three components: the anomalous advection by the zonal current, by the meridional current, and by the vertical current. In turn, each component comprises three subcomponents: the anomalous advection by the anomalous temperature and mean current, the anomalous advection by the mean temperature and anomalous current, and the nonlinear advection by the anomalous temperature and current. Figure 2b shows that the evolution of 15RCR between NPC2 and the anomalous total zonal advection is approximately positive, but it is insignificant before 1990. The positive correlation after 1990 suggests that this anomalous total advection is also a damping term for the CTM. Likewise, its component (the anomalous

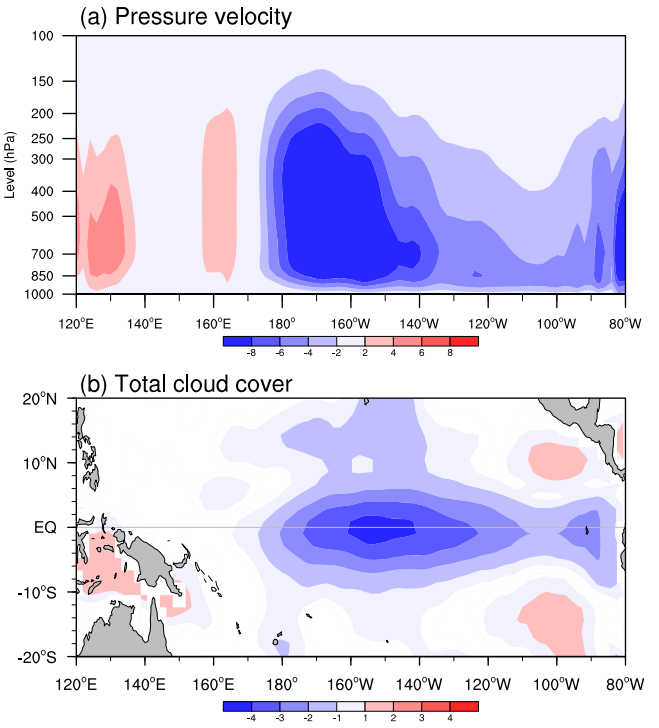

Figure 5. (a) Anomalies of pressure velocity (mean from 5°S to 5°N; -10^{-3} Pa s^{-1}) and (b) total cloud cover (%) regressed on NPC2 over the period 1960–2008. Shading indicates statistical significance at the 99% confidence level.

zonal advection of the anomalous temperature by the mean zonal current, $-\bar{u}\partial T'/\partial x$) is a damping term for the CTM (Figure 2b). However, the anomalous zonal advection of the mean temperature by the anomalous current ($-u'\partial\bar{T}/\partial x$) has a stable negative 15RCR with NPC2 (Figure 2b). This indicates that the $-u'\partial\bar{T}/\partial x$ term contributes to the temperature change associated with the CTM in the eastern equatorial Pacific. In addition, the 15RCR between NPC2 and the nonlinear zonal advection term ($-u'\partial T'/\partial x$) displays a stable positive correlation, indicating that $-u'\partial T'/\partial x$ is also a damping term.

In Figures 2c and 2d, the 15RCRs between NPC2 and the anomalous total meridional, as well as vertical advections, significantly contribute to the anomalous temperature change associated with the CTM in the eastern equatorial Pacific. In particular, the anomalous meridional advection of the anomalous temperature by the mean current ($-\bar{v}\partial T'/\partial y$), the anomalous vertical advection of the anomalous temperature by the mean upwelling ($-\bar{w}\partial T'/\partial z$), and the anomalous vertical advection of the mean temperature by the anomalous upwelling ($-w'\partial\bar{T}/\partial z$) show stable negative 15RCRs with NPC2. This finding indicates that these terms play an important role in the CTM-associated ocean temperature change. Additionally, the anomalous meridional advection of the mean temperature by the anomalous current ($-v'\partial\bar{T}/\partial y$) and the nonlinear meridional advection ($-v'\partial T'/\partial y$) are insignificant for the majority of the record and also are damping terms for the CTM (Figure 2c). The nonlinear vertical ($-w'\partial T'/\partial z$) advection displays an unstable relationship with the CTM (Figure 2d).

3.3. Main Ocean Dynamical Processes Associated With the CTM

The running correlation analysis of the temperature heat budget shows that the four anomalous advection terms ($-u'\partial\bar{T}/\partial x$, $-\bar{v}\partial T'/\partial y$, $-\bar{w}\partial T'/\partial z$, and $-w'\partial\bar{T}/\partial z$) play an important role in the temperature change associated with the CTM in the oceanic mixed layer of the eastern equatorial Pacific. Note that our sensitivity test with the running year changed from 10 to 25 years shows the same results. To examine how the anomalous advection terms impact the anomalous temperature tendency in the eastern equatorial Pacific, we regress the zonal mean anomalous temperature tendency and advection terms onto NPC2 over the period 1960–2008. Figures 6a and 6b indicate that the cooling temperature tendency can be broadly explained by the anomalous total advection term at the equator.

By comparing the anomalous total zonal advection (Figure 6c) with the temperature tendency (Figure 6a), it can be further demonstrated that the anomalous total zonal advection term is the damping term for the anomalous temperature tendency of the thermocline (generally at about 60 m in the eastern equatorial Pacific) related to the CTM from about 2°S to 2°N, while it makes some contribution to the anomalous cooling temperature tendency from about 6°S to 2°S, and from about 2°N to 6°N. The term $-\bar{u}\partial T'/\partial x$ exhibits a warm tendency in the thermocline from about 4°S to 4°N (Figure 6d). The accompanying anomalous zonal temperature gradient ($\partial T'/\partial x$) in the eastern equatorial Pacific region is positive in the 0–40 m layer (Figure 7a). Corresponding to the mean zonal current ($\bar{u}$) in the eastern equatorial Pacific region, the south equatorial current (SEC) is westward. This means the term $-\bar{u}\partial T'/\partial x$ corresponds to the warming temperature tendency in the eastern equatorial Pacific, but it plays a damping term in comparison with the anomalous temperature tendency of the CTM (Figure 6a).

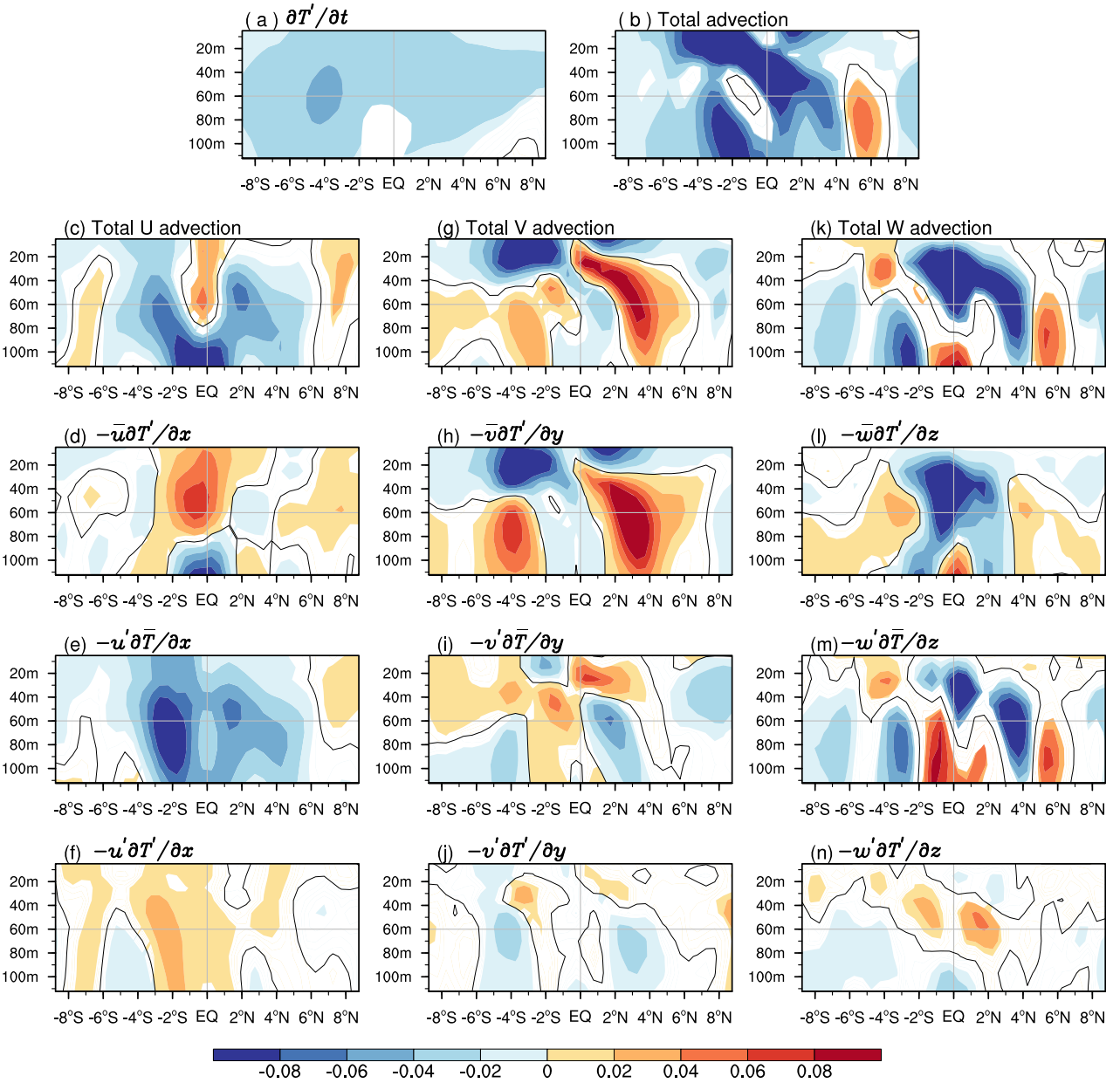

Figure 6. Regression of advection terms (10^{-6}°C s^{-1}) in the eastern tropical Pacific (140°W–80°W) onto NPC2 for the period 1960–2008. (a) Temperature tendency. (b) Total temperature advection. (c–f) Total zonal temperature advection, advection by the mean zonal current, advection by the anomalous zonal current, and the zonal nonlinear term, respectively. (g–j, k–n) As in Figures 6c–6f, but for the meridional and vertical temperature advections. In all parts, shading indicates statistical significance at the 99% confidence level, and the thin black contour denotes the zero line.

Nevertheless, the term $-u'\partial\bar{T}/\partial x$ contributes to the anomalous cooling temperature tendency in the whole thermocline of the eastern equatorial Pacific (Figure 6e). As the temperature is gradually cooling from west to east along the equatorial Pacific, the mean zonal temperature gradient ($\partial\bar{T}/\partial x$) is always negative. Associated with the positive CTM, there is an anomalous westward zonal current (u') in the total thermocline (Figure 8a), opposite in direction to the westerly wind stress anomalies in the eastern equatorial Pacific (Figure 4). This indicates that the anomalous zonal current associated with the CTM is not controlled solely by the wind stress anomalies (refer to Appendix A for details). Figure 9a shows the 15RCRs between NPC2 and the anomalous total zonal current (green line), the anomalous Ekman current (orange line), and the anomalous semigeostrophic current (blue line). The anomalous total zonal current related to the CTM depends mainly on the anomalous zonal semigeostrophic current, and it has a stable negative 15RCR with NPC2. Overall, when the CTM is in its positive phase, the thermocline uplift (the thermocline depth anomaly

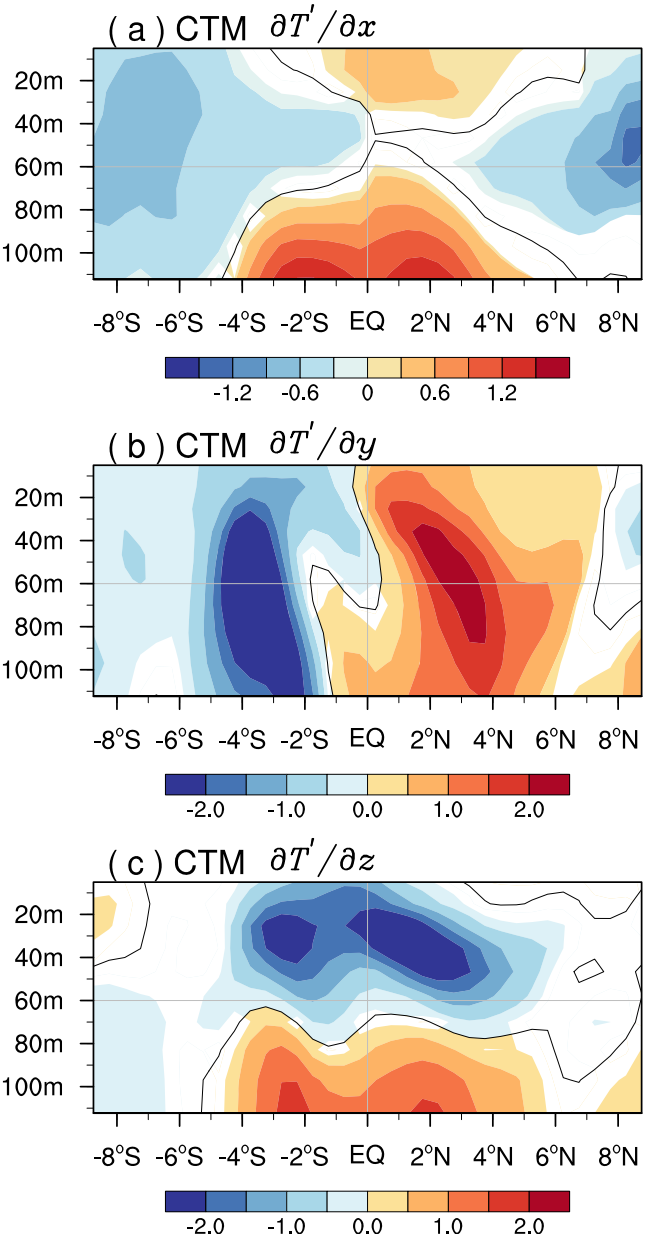

Figure 7. Anomalies of (a) zonal temperature gradient (10^{-7}°C m^{-1}), (b) meridional temperature gradient (10^{-6}°C m^{-1}), and (c) vertical temperature gradient (10^{-2}°C m^{-1}) in the eastern tropical Pacific (140°W–80°W) regressed on NPC2 over the period 1960–2008. In all parts, shading indicates the 99% confidence level, and the thin black contour denotes the zero line.

is referred to as TDA below; red line in Figure 9a) induces a westward anomalous zonal semigeostrophic current (blue line in Figure 9a) and thus contributes to the cooling term $-u'\partial\bar{T}/\partial x$ in the eastern equatorial Pacific. In addition, the nonlinear zonal advection term (Figure 6f) is weak and can be ignored.

The term $-\bar{v}\partial T'/\partial y$ depicts the cooling temperature tendency in the upper layer of the eastern equatorial Pacific when the CTM is in its positive phase (Figure 6h). This term is controlled by the anomalous meridional temperature gradient ($\partial T'/\partial y$). Figure 8d shows that the strongest latitudinal cooling temperature anomalies associated with the CTM are located in the equatorial region of the eastern Pacific, thus the term $\partial T'/\partial y$ in the upper layer is positive north of the equator but negative south of the equator (Figure 7b). In other words, the poleward anomalous temperature gradient ($\partial T'/\partial y$ (N–S)), which is obtained by subtracting the southern $\partial T'/\partial y$ term (2°S–0°S) from the northern $\partial T'/\partial y$ term (0°N–2°N), is positive. Meanwhile, this term $\partial T'/\partial y$ (N–S) maintains a stable relationship with the CTM (blue line in Figure 9c). In addition, the mean meridional current ($\bar{v}$) is divergent in the upper layer of the eastern equatorial Pacific [e.g., *Kessler et al.*, 1998; *McPhaden et al.*, 1998; *Zhang et al.*, 2009]. It is suggested that the corresponding terms $\partial T'/\partial y$ and $\bar{v}$ could induce the cooling term $-\bar{v}\partial T'/\partial y$. By comparing Figure 6g with 6h, the total meridional advection anomalies can be attributed mainly to the term $-\bar{v}\partial T'/\partial y$ in the eastern equatorial Pacific. The other two terms play only a minor role in the total meridional advection anomalies.

Although the term $-v'\partial\bar{T}/\partial y$ acts to damp the CTM (Figure 2c), it enhances the cooling tendency to the south of the equator and weakens the cooling tendency to the north of the equator in the 0–30 m layer (Figure 6i). As the mean temperature of the Pacific equator is cooler than that of the Pacific off-equator, the mean meridional temperature gradient ($\partial\bar{T}/\partial y$) is positive north of the equator but negative south of the equator. In addition, the corresponding anomalous meridional current (v') moves southward in the eastern equatorial Pacific (Figure 8b). Its direction is controlled primarily by the meridional wind stress anomalies (Figure 4). Similar to the anomalous zonal advections, the nonlinear meridional advection (Figure 6j) can also be ignored.

The anomalous total vertical advection also contributes to the anomalous temperature tendency associated with the CTM in the eastern equatorial Pacific (Figure 6a versus Figure 6k). Its component of the term $-\bar{w}\partial T'/\partial$

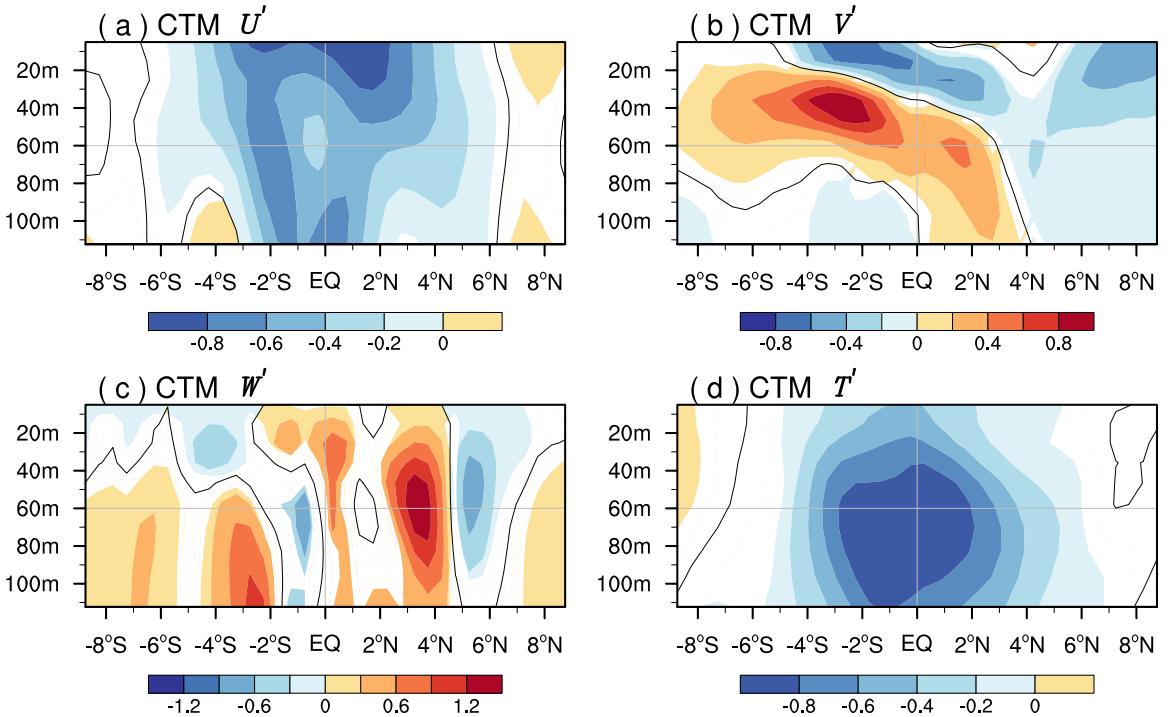

Figure 8. As in Figure 7, except for anomalous (a) zonal current (10^{-1} m s^{-1}), (b) meridional current (10^{-2} m s^{-1}), (c) vertical current (positive upward; 10^{-6} m s^{-1}), and (d) temperature (°C).

z cools the temperature tendency of the whole thermocline (Figure 6l). As the relative cooling center of temperature anomalies is located in the lower layer (Figure 8d), the vertical gradient of the temperature anomaly ($\partial T'/\partial z$) is negative over the whole thermocline (Figure 7c). This indicates an increasing temperature difference between the upper and lower layer of the ocean. Also, this temperature difference maintains a stable relationship with the CTM (red line in Figure 9c). When the negative term $\partial T'/\partial z$ is accompanied by the strong mean positive upwelling ($\bar{w}$), the term $-\bar{w}\partial T'/\partial z$ contributes to the cooling temperature tendency.

As the mean subsurface temperature is cooler than that at the surface, it is corresponding to the negative mean vertical gradient ($\partial \bar{T}/\partial z$). When the anomalous upwelling (w' in Figure 8c) is positive in the eastern equatorial Pacific, the term $-w'\partial \bar{T}/\partial z$ exhibits a cooling in ocean temperature tendency (Figure 6m). This begs the question, what induces the anomalous upwelling associated with the CTM? Figure 9b shows that the increasing SSTA gradient (red line) causes the decreasing SLP anomaly (SLPA) gradient (blue line) along the equatorial Pacific, when the CTM is in its positive phase. There is a strengthening anomalous divergence of meridional wind stress (referred to as Vs (N–S) below; orange line in Figure 9b), which has a strong correlation with the anomalous divergence in wind stress (above 0.98) over the eastern equatorial Pacific. As the Coriolis force is approximately equal to 0 at the equator, the anomalous divergence of meridional wind stress enhances the anomalous divergence of the Ekman currents (green line), and further increases the upwelling (purple line). However, this anomalous advection term plays a smaller role than the term $-w'\partial \bar{T}/\partial z$ in the eastern equatorial Pacific. The nonlinear vertical advection (Figure 6n) can also be ignored.

4. Relationships Between Ocean Dynamical Processes and Global Warming

The above results demonstrate that the four anomalous advections ($-u'\partial \bar{T}/\partial x$, $-\bar{v}\partial T'/\partial y$, $-\bar{w}\partial T'/\partial z$, and $-w'\partial \bar{T}/\partial z$) contribute to the cooling total advection anomalies in the whole thermocline of the eastern equatorial Pacific (Figure 6b), which furthermore induce the CTM-associated ocean temperature change (Figure 6a). Figure 10e (bottom) shows a normalized time series of the sum of these four anomalous advection terms (referred to below as the sum of anomalous cooling advection terms) in the whole thermocline. After removal of the ENSO (Nino3 index), the partial correlation coefficients (PRs) between the tropical Pacific temperature anomalies

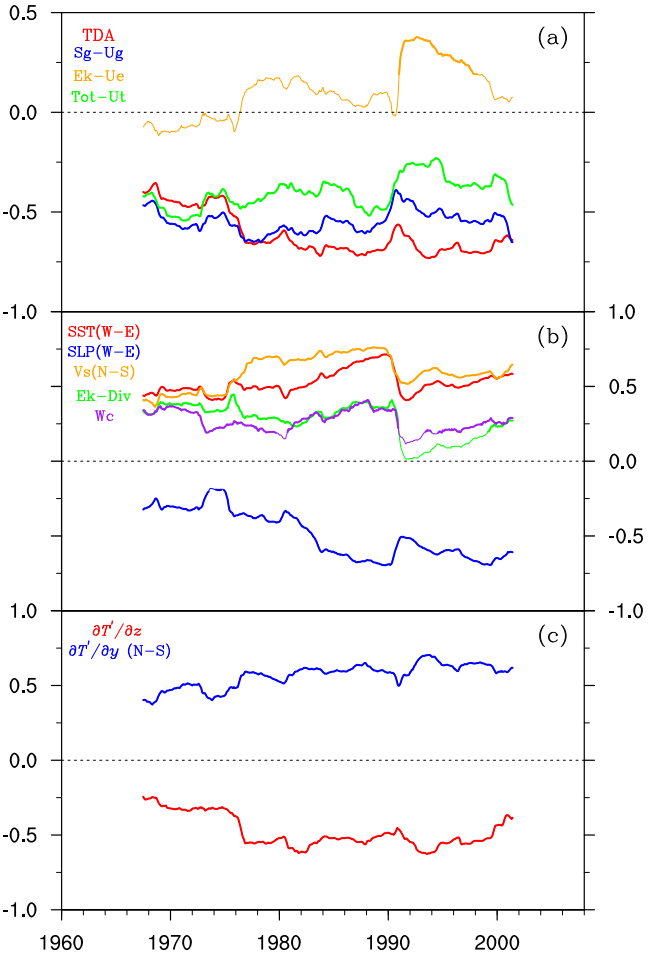

Figure 9. Time series of 15RCR between NPC2 and various terms related to the atmosphere and ocean. (a) Red, blue, orange, and green lines indicate the TDA (thermocline depth anomaly), the zonal semigeostrophic current, the zonal Ekman current, and the total zonal current, respectively. (b) Red, blue, orange, green, and purple lines indicate the zonal SSTA gradient (western-eastern), the zonal SLPA gradient (western-eastern), divergence of meridional wind stress (north-south; north: 0°N–2°N, south: 2°S–0°S), divergence of Ekman currents, and upwelling, respectively. (c) Red and blue lines indicate the vertical temperature gradient and poleward temperature gradient (north-south; north: 0°N–2°N, south: 2°S–0°S), respectively. Except for the area of zonal gradient of SSTA and SLPA (western: 5°S–5°N, 140°E–160°W; eastern: 5°S–5°N, 140°W–80°W), the calculated area of all terms is located in the eastern equatorial Pacific (2°S–2°N, 140°W–80°W, note that the oceanic term is from 0 to 30 m). Thicker lines indicate the 99% confidence level.

(averaged over 0–60 m) and the sum of anomalous cooling advection terms correspond to the negative correlation (multiplied by −1.0) over the tropical Pacific cold tongue region (Figure 10e). This result suggests that the temperature anomalies show a cooling change when the sum of anomalous cooling advection terms is negative. This spatial pattern of PRs (Figure 10e) is similar to the spatial pattern of the CTM (Figure 1), which represents the out-of-phase relationship in SSTA variability between the Pacific cold tongue region and elsewhere in the tropical Pacific.

Furthermore, *Zhang et al.* [2010] argued that the CTM's long-term change is most probably induced by ocean dynamical processes in response to global warming. Table 1 lists the PRs between the sum of anomalous cooling advection terms and the CTM and global warming, which are all significant at the 99% confidence level. In addition, the time series of the sum of anomalous cooling advection terms has a significantly negative trend (−0.33 per 30 years; Table 1). This suggests that the sum of anomalous cooling advection terms is the main contributor to the long-term change in the CTM. Thus, it is necessary to examine whether the four components ($-u'\partial\bar{T}/\partial x$, $-\bar{v}\partial T'/\partial y$, $-\bar{w}\partial T'/\partial z$, and $-w'\partial\bar{T}/\partial z$) respond to global warming and contribute to the long-term change in the CTM.

Table 1 also shows the 30 year trends of the time series of four anomalous ocean advections. They all follow a negative trend, suggesting that each term plays a role in the long-term change of the CTM. However, only the term $-\bar{w}\partial T'/\partial z$ displays a strong negative trend (−0.74 per 30 years; Table 1) and exceeds the 95% confidence level. The normalized time series of the term $-\bar{w}\partial T'/\partial z$ is in an almost positive phase in the pre-1980 period, but an almost negative phase in the post-1980 period (Figure 10a, bottom). The negative PRs between the term $-\bar{w}\partial T'/\partial z$ and the CTM and global warming are all significant at the 99% confidence level and are strongest among the four anomalous advection terms (Table 1). Figure 10a (top) shows the PRs between the anomalous tropical Pacific temperature and the term $-\bar{w}\partial T'/\partial z$. This corresponds to the negative correlation over the tropical Pacific cold tongue region, where the cooling anomalous $-\bar{w}\partial T'/\partial z$ term is associated with the negative temperature anomalies. As mentioned above, the term $-\bar{w}\partial T'/\partial z$ is closely related to the long-term change of the CTM under global warming.

The long-term change of the term $-\bar{w}\partial T'/\partial z$ is controlled by the decreasing vertical gradient of temperature anomalies ($\partial T'/\partial z$; Figure 11a), whose trend is −0.01 per 30 years at the 95% confidence level over the period 1960–2008. There are also significant PRs between the term $\partial T'/\partial z$ and the CTM (about −0.46) and global

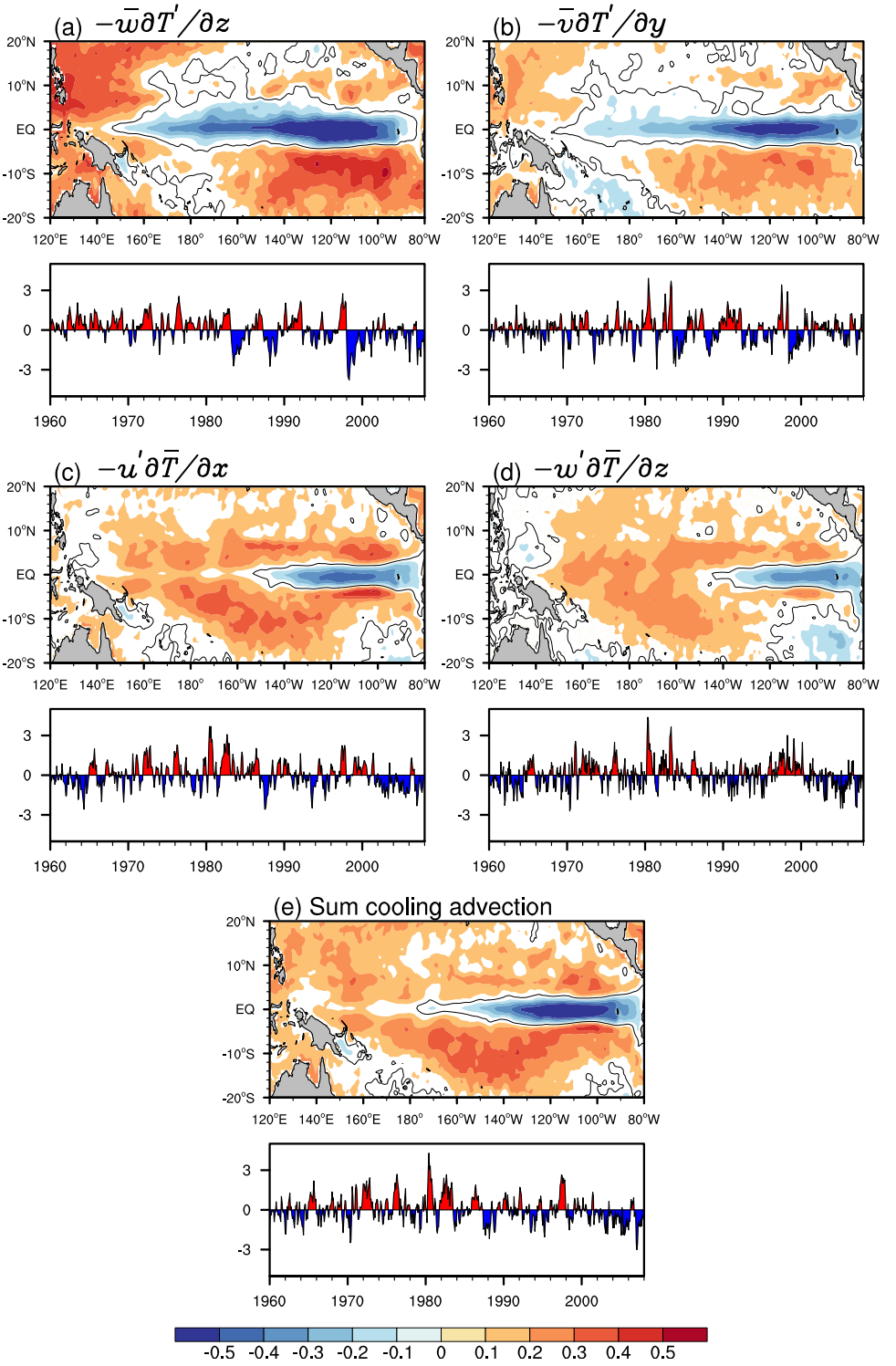

Figure 10. (top) Partial correlation coefficients (after removal of ENSO) between the tropical Pacific oceanic temperature (0–60 m) and the monthly indices of (a–d) four cooling ocean advections and (e) the sum cooling advection. (bottom) The corresponding normalized time series of the indices. These indices are calculated over 2°S–2°N, 140°W–80°W, and 0–60 m. Shading indicates statistical significance at the 99% confidence level, and the thin black contour denotes the zero line. To allow a direct comparison, the PR patterns in Figures 10a–10e are multiplied by −1.0.

Table 1. Partial Correlation Coefficients (After Removal of ENSO) Between Time Series of Ocean Advections and NPC2 (First Row) and the Global Warming Index (GWI; Second Row)[a]

	$-\bar{w}\partial T'/\partial z$	$-\bar{v}\partial T'/\partial y$	$-u'\partial\bar{T}/\partial x$	$-w'\partial\bar{T}/\partial z$	Sum Cooling Advection
NPC2	**−0.47**	**−0.21**	**−0.27**	**−0.17**	**−0.38**
GMI	**−0.41**	−0.08	**−0.19**	**−0.13**	**−0.29**
Trend	**−0.74**	−0.06	−0.14	−0.01	**−0.33**

[a]The 30 year trends of ocean advections (third row) for the time series are also shown. These indices of ocean advections are calculated over 2°S–2°N, 140°W–80°W, and 0–60 m. The GWI is the HadCRUT4 global mean surface temperature. (Bold values indicate significant at the 99% confidence level (Student's *t* test) or at the 95% confidence level (nonparametric Mann-Kendall test).)

warming (about −0.44). We can regard the surface and subsurface temperatures as their climate mean state in the initial period. Suppose a uniform external heating, which can be thought of as global warming, is imposed on the tropical Pacific. In the eastern equatorial Pacific, the SST will tend to increase, but the subsurface temperature is not affected, which leads the term $\partial T'/\partial z$ toward the negative anomaly. The negative $\partial T'/\partial z$ term accompanied by the mean upwelling ($\bar{w}$; i.e., the cooling term $-\bar{w}\partial T'/\partial z$) could induce the cooling temperature (Figure 8d) in the eastern equatorial Pacific. In addition, the center of the term $-\bar{w}\partial T'/\partial z$ is located in the subsurface (Figure 6l), indicating that this term could also increase the difference between the subsurface and surface temperature (i.e., the decreasing term $\partial T'/\partial z$; Figure 7c) in the eastern equatorial Pacific.

The cooling eastern equatorial Pacific temperature could induce an increased poleward temperature gradient, uplifted thermocline depth, and strengthened divergence of meridional wind stress, which is expected to induce the three cooling advections ($-\bar{v}\partial T'/\partial y$, $-u'\partial\bar{T}/\partial x$, and $-w'\partial\bar{T}/\partial z$). Figures 10b–10d (top) and Figures 11b–11d (top) respectively show the PRs between the anomalous tropical Pacific temperature and these terms ($-\bar{v}\partial T'/\partial y$, $-u'\partial\bar{T}/\partial x$, and $-w'\partial\bar{T}/\partial z$; $\partial T'/\partial y$ (N–S), TDA, and Vs (N–S)). The spatial patterns of all PRs show negative correlations over the tropical Pacific cold tongue region, similar to the spatial pattern of the CTM. Although most of the PRs between these three advection terms and the CTM or global warming are significant, no significant trend is detected (Table 1). This means they make a minor contribution to the long-term change in the CTM.

5. Discussion and Conclusions

The CTM [*Zhang et al.*, 2010] represents the out-of-phase relationship in SSTA variability between the Pacific cold tongue region and elsewhere in the tropical Pacific. The long-term change in the CTM is likely related to global warming [*Cane et al.*, 1997; *Zhang et al.*, 2010]. Using a heat budget analysis of the ocean temperature in the eastern equatorial Pacific, it is found that the net heat flux is a damping term and that the four anomalous advections ($-u'\partial\bar{T}/\partial x$, $-\bar{v}\partial T'/\partial y$, $-\bar{w}\partial T'/\partial z$, and $-w'\partial\bar{T}/\partial z$) play an important role in the CTM-associated temperature variability. However, only the term $-\bar{w}\partial T'/\partial z$ displays a strong decreasing trend, which is closely related to the long-term change in the CTM. Note that these results are also obtained when NPC2 is generated from the ERSST v3b, COBE2, and Kaplan data sets (supporting information Figures S1–S16 and Table S1). Despite the uncertainties of SODA 2.2.4 data set in the early period (1871–1900), we obtain the same results both in the period 1871–2008 and in the period 1900–2008 (supporting information Figure S17–S28 and Table S1), which is also the same with the results from the other four data sets (HadISST1, ERSST v3b, COBE2, and Kaplan). It is suggested that our results are not sensitive to the different instrumental SST reconstruction.

The long-term change of the cooling $-\bar{w}\partial T'/\partial z$ term depends on the decreasing vertical gradient of the temperature anomaly ($\partial T'/\partial z$). In fact, suppose a uniform external heating, which can be regarded as global warming, is imposed on the tropical Pacific. In the eastern equatorial Pacific, the SST will tend to increase, but the subsurface ocean temperature is not affected, which causes the anomalous vertical temperature gradient ($\partial T'/\partial z$) to move toward a negative anomaly. The accompanying mean upwelling ($\bar{w}$) induces the anomalous vertical advection term ($-\bar{w}\partial T'/\partial z$), which makes a contribution to the cooling surface temperature and the decreasing vertical temperature gradient in the eastern equatorial Pacific. The decreasing vertical temperature gradient further enhances the cooling $-\bar{w}\partial T'/\partial z$ term, which is likely to be a negative feedback in response to the forcing of global warming. Subsequently, the cooling temperature leads to an increased poleward temperature gradient, uplifted thermocline depth, and strengthened divergence of meridional wind stress. These three terms are expected to further induce the cooling advection terms ($-\bar{v}\partial T'/\partial y$, $-u'\partial\bar{T}/\partial x$, and $-w'\partial\bar{T}/\partial z$), and thus these three cooling advection terms can also make a contribution to the cooling

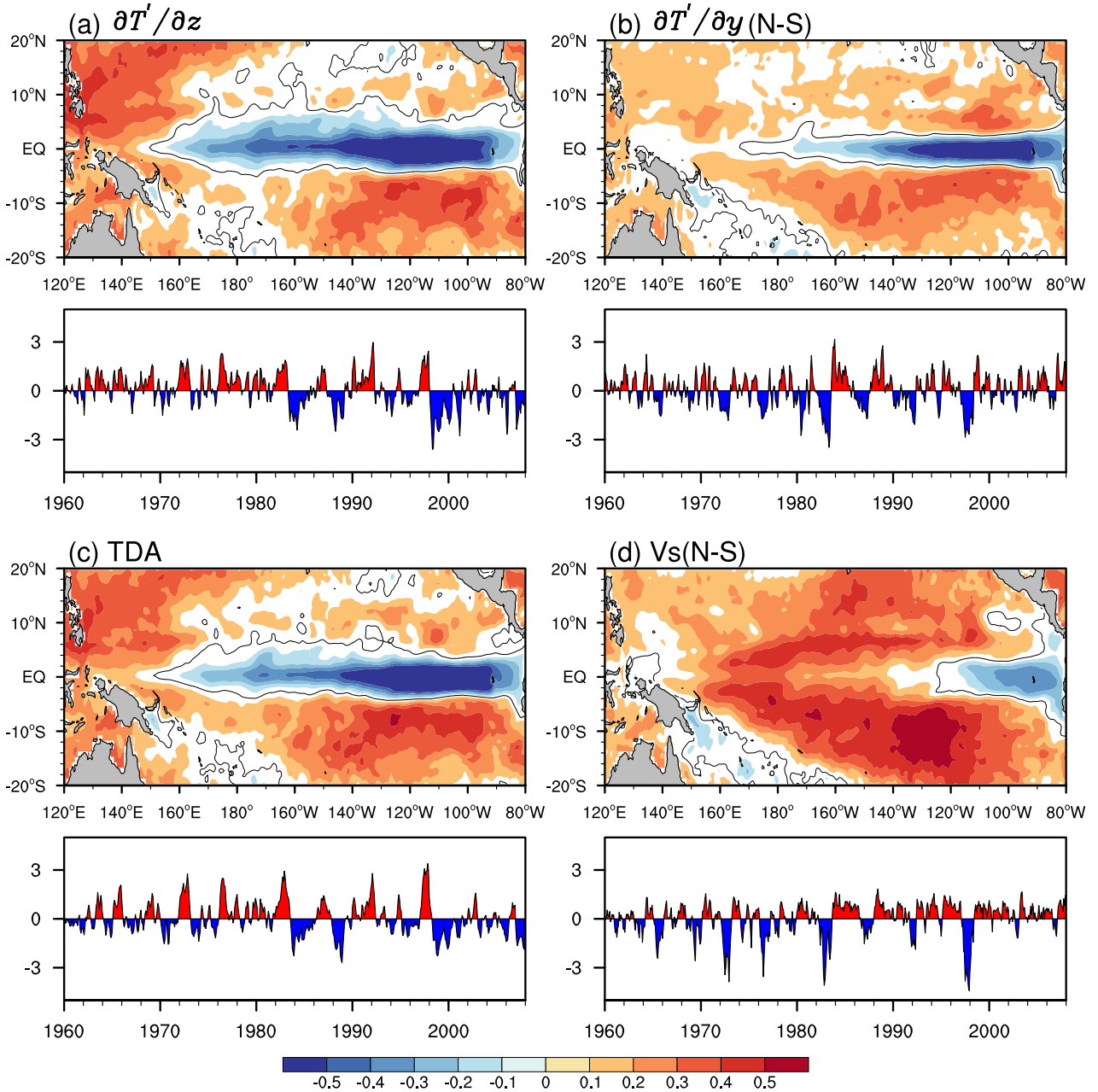

Figure 11. As in Figure 10, except for (a) the vertical temperature gradient, (b) the poleward temperature gradient, (c) TDA, and (d) Vs (N–S) indices. To allow a direct comparison, the PR patterns in Figures 11a and 11c are multiplied by −1.0.

temperature. Although these three oceanic dynamic processes' long-term trends are cooling, no significant trends are detected. It is suggested that only one term ($-\bar{w}\partial T'/\partial z$), which represents the increased ocean thermal stratification, makes a major contribution to the long-term cooling change of oceanic temperature in the eastern equatorial Pacific. This result is consistent with *DiNezio et al.* [2009], while it differs from the associated ocean dynamical feedback presented by *Cane et al.* [1997], in which both the anomalous vertical advection of the anomalous temperature by the mean upwelling and advection of the mean temperature by the anomalous upwelling ($-\bar{w}\partial T'/\partial z$ and $-w'\partial \bar{T}/\partial z$) are emphasized.

Yang et al. [2014] depicted a historical strengthening of the Pacific subtropical cells (STCs) in the Simple Ocean Data Assimilation-sparse input version 1 (SODAsi.1) and reported a cooling trend over the central tropical Pacific (their Figure 2). Note that this cooling region in *Yang et al.* [2014] overlaps in part with the

positive CTM's cooling region. In addition, anomalous easterlies occur in the west of the cooling region and anomalous westerlies in the east. These anomalous easterlies accelerate the STC and thus increase the transport of water between the subtropical and equatorial thermocline. As the CTM is in its positive phase, strong easterly anomalies appear west of about 140°W, and weak westerly anomalies occur east of about 140°W (Figure 4). These easterly anomalies associated with the CTM may contribute to the accelerated STC.

Drenkard and Karnauskas [2014] used the SODA 2.2.6 data set to investigate historical strengthening of the Pacific equatorial undercurrent (EUC). As the zonal wind stress increases along the Pacific equator, the zonal pressure gradient force is strengthened and thus the EUC is increased [*Drenkard and Karnauskas*, 2014]. This means that the easterly anomalies associated with the CTM may also contribute to the historical strengthening of the EUC. Simultaneously, the strengthening STC and EUC would transport more cold water to the eastern equatorial thermocline. This is accompanied by the mean positive upwelling, and the anomalous advection by the mean upwelling ($-\bar{w}\partial T'/\partial z$) may make a contribution to the cooling temperature tendency (or CTM) in the eastern equatorial Pacific. Overall, the historical strengthening of the STC and EUC is likely related to the CTM. In addition, the cooling eastern equatorial Pacific thermocline is detected not only in the SODA data set but also in the subsurface temperature of Ishii and ORAS4 data sets (not shown).

This paper demonstrates that the long-term variability in the CTM is most probably induced by ocean dynamical processes in response to global warming. *Zhang et al.* [2010] used the Phase 3 of the Coupled Model Intercomparison Project (CMIP3) models to investigate the second EOF modes under the twentieth century run (20C3M) and preindustrial control (picntrl) scenario, in which there is no forcing by global warming. Under both the 20C3M and picntrl scenarios of the CMIP3 models, the corresponding spatial patterns of the second EOF mode show cooling SSTA in the tropical Pacific cold tongue region [*Zhang et al.*, 2010, Figures 7 and 12b]. The corresponding principal components of the second EOF mode exhibit a clearly long-term change under the 20C3M scenario, whereas they show an interannual variability under the picntrl scenario. In Phase 5 of CMIP's historical simulation and preindustrial control (piControl) scenario, the second EOF mode over the tropical Pacific is also investigated (not shown). The spatial and temporal features of these second EOF modes are consistent with those of CMIP3. It is suggested that the CTM is an interannual variability mode under the preindustrial control scenario, but it will become the long-term cold trend mode through ocean dynamic processes in response to global warming. In future work, we intend to carry out further research into the ocean dynamical mechanism of the CTM under the different scenarios of CMIP3 and CMIP5, and this should help to more clearly understand the background climate change over the tropical Pacific, the possible influence on El Niño regime change, and the preexisting and future hiatus periods [e.g., *Kosaka and Xie*, 2013; *Li et al.*, 2013; *England et al.*, 2014; *Meehl et al.*, 2014] under global warming.

Appendix A: Anomalous Ekman Currents and Semigeostrophic Currents

We use an equatorial β-plane framework to diagnose wind-induced Ekman currents and semigeostrophic currents in the equatorial Pacific. The anomalous zonal and meridional Ekman currents (u_e and v_e, respectively) and semigeostrophic currents (u_g and v_g, respectively) can be written as follows [e.g., *Chang and Philander*, 1994; *Su et al.*, 2010, 2014]:

$$u_e = \frac{1}{\rho \bar{H}} \frac{r_s \tau^x + \beta y \tau^y}{r_s^2 + (\beta y)^2} \tag{A1}$$

$$v_e = \frac{1}{\rho \bar{H}} \frac{r_s \tau^y - \beta y \tau^x}{r_s^2 + (\beta y)^2} \tag{A2}$$

$$u_g = -\frac{g'}{\beta} \frac{\partial^2 h}{\partial y^2} \tag{A3}$$

$$v_g = \frac{g'}{\beta} \frac{\partial^2 h}{\partial x \partial y} \tag{A4}$$

where ρ is the density of seawater; $\bar{H} = 30$ m is the mean mixed layer depth; τ^x and τ^y are the anomalous zonal and meridional wind stress, respectively; r_s is the dissipation rate; g' is the reduced gravity; β is the planetary vorticity gradient; and h is the anomalous thermocline depth (the mean thermocline depth is the depth of the 20°C isotherm).

Acknowledgments
We thank Kristopher Karnauskas for constructive comments and suggestions. We also acknowledge the helpful suggestions and comments of two anonymous reviewers. This work was jointly supported by the National Natural Science Foundation of China (grants 41375110 and 41475076). The SODA data set was obtained from the National Center for Atmospheric Research (NCAR) and can be downloaded from http://dsrs.atmos.umd.edu/DATA/soda_2.2.4/. The 20CR2 data set was obtained from the National Oceanic and Atmospheric Administration (NOAA) and is available at http://www.esrl.noaa.gov/psd/data/gridded/data.20thC_ReanV2.monolevel.mm.html. The HadISST1 and HadCRUT4 data sets were obtained from the Met Office Hadley Centre and can be downloaded from http://www.metoffice.gov.uk/hadobs/hadisst/data/download.html and http://www.cru.uea.ac.uk/cru/data/temperature/, respectively.

References

Ashok, K., S. K. Behera, S. A. Rao, H. Y. Weng, and T. Yamagata (2007), El Niño Modoki and its possible teleconnection, *J. Geophys. Res.*, *112*, C11007, doi:10.1029/2006JC003798.

Cai, W. J., and T. Cowan (2009), La Niña Modoki impacts Australia autumn rainfall variability, *Geophys. Res. Lett.*, *36*, L12805, doi:10.1029/2009GL037885.

Cai, W. J., and P. H. Whetton (2000), Evidence for a time-varying pattern of greenhouse warming in the Pacific Ocean, *Geophys. Res. Lett.*, *27*(16), 2577–2580, doi:10.1029/1999GL011253.

Cane, M. A. (1998), Climate change—A role for the tropical Pacific, *Science*, *282*(5386), 59–61, doi:10.1126/science.282.5386.59.

Cane, M. A., A. C. Clement, A. Kaplan, Y. Kushnir, D. Pozdnyakov, R. Seager, S. E. Zebiak, and R. Murtugudde (1997), Twentieth-century sea surface temperature trends, *Science*, *275*(5302), 957–960, doi:10.1126/science.275.5302.957.

Carton, J. A., and B. S. Giese (2008), A reanalysis of ocean climate using Simple Ocean Data Assimilation (SODA), *Mon. Weather Rev.*, *136*(8), 2999–3017.

Chang, P., and S. G. Philander (1994), A coupled ocean–atmosphere instability of relevance to the seasonal cycle, *J. Atmos. Sci.*, *51*(24), 3627–3648.

Choi, J., S. I. An, J. S. Kug, and S. W. Yeh (2011), The role of mean state on changes in El Niño's flavor, *Clim. Dyn.*, *37*(5–6), 1205–1215, doi:10.1007/s00382-010-0912-1.

Clement, A. C., R. Seager, M. A. Cane, and S. E. Zebiak (1996), An ocean dynamical thermostat, *J. Clim.*, *9*(9), 2190–2196.

Collins, M., et al. (2010), The impact of global warming on the tropical Pacific ocean and El Niño, *Nat. Geosci.*, *3*(6), 391–397, doi:10.1038/ngeo868.

Compo, G. P., and P. D. Sardeshmukh (2010), Removing ENSO-related variations from the climate record, *J. Clim.*, *23*(8), 1957–1978.

Compo, G. P., et al. (2011), The twentieth century reanalysis project, *Q. J. R. Meteorol. Soc.*, *137*(654), 1–28, doi:10.1002/qj.776.

DiNezio, P. N., A. C. Clement, G. A. Vecchi, B. J. Soden, and B. P. Kirtman (2009), Climate response of the equatorial pacific to global warming, *J. Clim.*, *22*(18), 4873–4892.

Drenkard, E. J., and K. B. Karnauskas (2014), Strengthening of the Pacific equatorial undercurrent in the SODA reanalysis: Mechanisms, ocean dynamics, and implications, *J. Clim.*, *27*(6), 2405–2416.

Duan, W. S., B. Tian, and H. Xu (2014), Simulations of two types of El Niño events by an optimal forcing vector approach, *Clim. Dyn.*, *43*(5–6), 1677–1692, doi:10.1007/s00382-013-1993-4.

England, M. H., S. McGregor, P. Spence, G. A. Meehl, A. Timmermann, W. J. Cai, A. Sen Gupta, M. J. McPhaden, A. Purich, and A. Santoso (2014), Recent intensification of wind-driven circulation in the Pacific and the ongoing warming hiatus, *Nat. Clim. Change*, *4*(3), 222–227, doi:10.1038/nclimate2106.

Fedorov, A. V., and S. G. Philander (2000), Is El Niño changing?, *Science*, *288*(5473), 1997–2002, doi:10.1126/science.288.5473.1997.

Feng, J., and J. P. Li (2011), Influence of El Niño Modoki on spring rainfall over south China, *J. Geophys. Res.*, *116*, D13102, doi:10.1029/2010JD015160.

Graham, N. E. (1995), Simulation of recent global temperature trends, *Science*, *267*(5198), 666–671, doi:10.1126/science.267.5198.666.

Held, I. M., and B. J. Soden (2006), Robust responses of the hydrological cycle to global warming, *J. Clim.*, *19*(21), 5686–5699.

Jin, F. F., Z. Z. Hu, M. Latif, L. Bengtsson, and E. Roeckner (2001), Dynamical and cloud-radiation feedbacks in El Niño and greenhouse warming, *Geophys. Res. Lett.*, *28*(8), 1539–1542, doi:10.1029/2000GL012078.

Kang, I. S., S. I. An, and F. F. Jin (2001), A systematic approximation of the SST anomaly equation for ENSO, *J. Meteorol. Soc. Jpn.*, *79*(1), 1–10.

Kao, H. Y., and J. Y. Yu (2009), Contrasting eastern-Pacific and central-Pacific types of ENSO, *J. Clim.*, *22*(3), 615–632.

Karnauskas, K. B., R. Seager, A. Kaplan, Y. Kushnir, and M. A. Cane (2009), Observed strengthening of the zonal sea surface temperature gradient across the equatorial Pacific Ocean, *J. Clim.*, *22*(16), 4316–4321.

Kessler, W. S., L. M. Rothstein, and D. K. Chen (1998), The annual cycle of SST in the eastern tropical Pacific, diagnosed in an ocean GCM, *J. Clim.*, *11*(5), 777–799.

Knutson, T. R., and S. Manabe (1995), Time–mean response over the tropical Pacific to increased CO_2 in a coupled ocean–atmosphere model, *J. Clim.*, *8*(9), 2181–2199.

Knutson, T. R., and S. Manabe (1998), Model assessment of decadal variability and trends in the tropical Pacific Ocean, *J. Clim.*, *11*(9), 2273–2296.

Kosaka, Y., and S. P. Xie (2013), Recent global-warming hiatus tied to equatorial Pacific surface cooling, *Nature*, *501*(7467), 403–407, doi:10.1038/nature12534.

Krueger, O., F. Schenk, F. Feser, and R. Weisse (2013), Inconsistencies between long-term trends in storminess derived from the 20CR reanalysis and observations, *J. Clim.*, *26*(3), 868–874.

Kug, J. S., F. F. Jin, and S. I. An (2009), Two types of El Niño events: cold tongue El Niño and warm pool El Niño, *J. Clim.*, *22*(6), 1499–1515.

Li, J. P., C. Sun, and F. F. Jin (2013), NAO implicated as a predictor of Northern Hemisphere mean temperature multidecadal variability, *Geophys. Res. Lett.*, *40*, 5497–5502, doi:10.1002/2013GL057877.

L'Heureux, M. L., S. Lee, and B. Lyon (2013), Recent multidecadal strengthening of the Walker circulation across the tropical Pacific, *Nat. Clim. Change*, *3*(6), 571–576, doi:10.1038/nclimate1840.

McPhaden, M. J., et al. (1998), The tropical ocean global atmosphere observing system: A decade of progress, *J. Geophys. Res.*, *103*(C7), 14,169–14,240, doi:10.1029/97JC02906.

McPhaden, M. J., S. E. Zebiak, and M. H. Glantz (2006), ENSO as an integrating concept in Earth science, *Science*, *314*(5806), 1740–1745, doi:10.1126/science.1132588.

Meehl, G. A., and W. M. Washington (1996), El Niño-like climate change in a model with increased atmospheric CO_2 concentrations, *Nature*, *382*(6586), 56–60, doi:10.1038/382056a0.

Meehl, G. A., H. Teng, and J. M. Arblaster (2014), Climate model simulations of the observed early-2000s hiatus of global warming, *Nat. Clim. Change*, *4*(10), 898–902, doi:10.1038/nclimate2357.

Morice, C. P., J. J. Kennedy, N. A. Rayner, and P. D. Jones (2012), Quantifying uncertainties in global and regional temperature change using an ensemble of observational estimates: The HadCRUT4 data set, *J. Geophys. Res.*, *117*, D08101, doi:10.1029/2011JD017187.

Noda, A., K. Yoshimatsu, S. Yukimoto, K. Yamaguchi, and S. Yamaki (1999), Relationship between natural variability and CO_2-induced warming pattern: MRI AOGCM experiment, paper presented at 10th Symposium on Global Change Studies, Am. Meteorol. Soc., Dallas, Tex.

Philander, S. G. H. (1990), *El Niño, La Niña, and the Southern Oscillation*, 293 pp., Academic, San Diego, Calif.

Rasmusson, E. M., and T. H. Carpenter (1982), Variations in tropical sea-surface temperature and surface wind fields associated with the southern oscillation El Niño, *Mon. Weather Rev.*, *110*(5), 354–384.

Rayner, N. A., D. E. Parker, E. B. Horton, C. K. Folland, L. V. Alexander, D. P. Rowell, E. C. Kent, and A. Kaplan (2003), Global analyses of sea surface temperature, sea ice, and night marine air temperature since the late nineteenth century, *J. Geophys. Res.*, *108*(D14), 4407, doi:10.1029/2002JD002670.

Ren, H. L., and F. F. Jin (2013), Recharge oscillator mechanisms in two types of ENSO, *J. Clim.*, *26*(17), 6506–6523.

Roeckner, E., J. M. Oberhuber, A. Bacher, M. Christoph, and I. Kirchner (1996), ENSO variability and atmospheric response in a global coupled atmosphere–ocean GCM, *Clim. Dyn.*, *12*(11), 737–754, doi:10.1007/s003820050140.

Seager, R., and R. Murtugudde (1997), Ocean dynamics, thermocline adjustment, and regulation of tropical SST, *J. Clim.*, *10*(3), 521–534.

Shinoda, T., H. E. Hurlburt, and E. J. Metzger (2011), Anomalous tropical ocean circulation associated with La Niña Modoki, *J. Geophys. Res.*, *116*, C12001, doi:10.1029/2011JC007304.

Solomon, A., and M. Newman (2012), Reconciling disparate twentieth-century Indo-Pacific ocean temperature trends in the instrumental record, *Nat. Clim. Change*, *2*(9), 691–699, doi:10.1038/nclimate1591.

Su, J. Z., R. H. Zhang, T. Li, X. Y. Rong, J. S. Kug, and C. C. Hong (2010), Causes of the El Niño and La Niña amplitude asymmetry in the equatorial eastern Pacific, *J. Clim.*, *23*(3), 605–617.

Su, J. Z., T. Li, and R. H. Zhang (2014), The initiation and developing mechanisms of central Pacific El Niño, *J. Clim.*, *27*(12), 4473–4485.

Sun, D. Z., and Z. Y. Liu (1996), Dynamic ocean–atmosphere coupling: A thermostat for the tropics, *Science*, *272*(5265), 1148–1150, doi:10.1126/science.272.5265.1148.

Taschetto, A. S., and M. H. England (2009), El Niño Modoki impacts on Australian rainfall, *J. Clim.*, *22*(11), 3167–3174.

Tett, S. (1995), Simulation of El Niño–Southern Oscillation-like variability in a global AOGCM and its response to CO_2 increase, *J. Clim.*, *8*(6), 1473–1502.

Timmermann, A., J. Oberhuber, A. Bacher, M. Esch, M. Latif, and E. Roeckner (1999), Increased El Niño frequency in a climate model forced by future greenhouse warming, *Nature*, *398*(6729), 694–697, doi:10.1038/19505.

Trenberth, K. E. (1997), The definition of El Nino, *Bull. Am. Meteorol. Soc.*, *78*(12), 2771–2777.

Trenberth, K. E., and T. J. Hoar (1996), The 1990–1995 El Niño Southern Oscillation event: Longest on record, *Geophys. Res. Lett.*, *23*(1), 57–60, doi:10.1029/95GL03602.

Vecchi, G. A., and B. J. Soden (2007), Global warming and the weakening of the tropical circulation, *Bull. Am. Meteorol. Soc.*, *88*(10), 1529–1530.

Vecchi, G. A., B. J. Soden, A. T. Wittenberg, I. M. Held, A. Leetmaa, and M. J. Harrison (2006), Weakening of tropical Pacific atmospheric circulation due to anthropogenic forcing, *Nature*, *441*(7089), 73–76, doi:10.1038/nature04744.

Vecchi, G. A., A. Clement., and B. J. Soden. (2008), Examining the tropical Pacific's response to global warming, *Eos Trans. AGU*, *89*(9), 81–83, doi:10.1029/2008EO090002.

Wang, B. (1995), Interdecadal changes in El Niño onset in the last 4 decades, *J. Clim.*, *8*(2), 267–285.

Wang, C. Z., and X. Wang (2013), Classifying El Niño Modoki I and II by different impacts on rainfall in Southern China and typhoon tracks, *J. Clim.*, *26*(4), 1322–1338.

Weng, H. Y., K. Ashok, S. K. Behera, S. A. Rao, and T. Yamagata (2007), Impacts of recent El Niño Modoki on dry/wet conditions in the Pacific rim during boreal summer, *Clim. Dyn.*, *29*(2–3), 113–129, doi:10.1007/s00382-007-0234-0.

Weng, H. Y., S. K. Behera, and T. Yamagata (2009), Anomalous winter climate conditions in the Pacific rim during recent El Niño Modoki and El Niño events, *Clim. Dyn.*, *32*(5), 663–674, doi:10.1007/s00382-008-0394-6.

Xiang, B. Q., B. Wang, and T. Li (2013), A new paradigm for the predominance of standing central Pacific warming after the late 1990s, *Clim. Dyn.*, *41*(2), 327–340, doi:10.1007/s00382-012-1427-8.

Yang, C. X., B. S. Giese, and L. X. Wu (2014), Ocean dynamics and tropical Pacific climate change in ocean reanalyses and coupled climate models, *J. Geophys. Res.*, *119*, 7066–7077, doi:10.1002/2014JC009979.

Yeh, S. W., J. S. Kug, B. Dewitte, M. H. Kwon, B. P. Kirtman, and F. F. Jin (2009), El Niño in a changing climate, *Nature*, *461*(7263), 511–570, doi:10.1038/nature08316.

Zebiak, S. E., and M. A. Cane (1987), A Model El Niño Southern Oscillation, *Mon. Weather Rev.*, *115*(10), 2262–2278.

Zhang, W. J., J. P. Li, and F. F. Jin (2009), Spatial and temporal features of ENSO meridional scales, *Geophys. Res. Lett.*, *36*, L15605, doi:10.1029/2009GL038672.

Zhang, W. J., J. P. Li, and X. Zhao (2010), Sea surface temperature cooling mode in the Pacific cold tongue, *J. Geophys. Res.*, *115*, C12042, doi:10.1029/2010JC006501.

Zhang, W. J., F. F. Jin, J. P. Li, and H. L. Ren (2011), Contrasting impacts of two-type El Niño over the western north Pacific during boreal autumn, *J. Meteorol. Soc. Jpn.*, *89*(5), 563–569.

Zhang, W. J., F. F. Jin, J. X. Zhao, L. Qi, and H. L. Ren (2013a), The possible influence of a nonconventional El Niño on the severe autumn drought of 2009 in southwest China, *J. Clim.*, *26*(21), 8392–8405.

Zhang, W. J., F. F. Jin, J. X. Zhao, and J. P. Li (2013b), On the bias in simulated ENSO SSTA meridional widths of CMIP3 models, *J. Clim.*, *26*(10), 3173–3186.

Zhang, W. J., L. Wang, B. Q. Xiang, L. Qi, and J. H. He (2014a), Impacts of two types of La Niña on the NAO during boreal winter, *Clim. Dyn.*, *44*(5), 1351–1366, doi:10.1007/s00382-014-2155-z.

Zhang, W. J., F. F. Jin, and A. Turner (2014b), Increasing autumn drought over southern China associated with ENSO regime shift, *Geophys. Res. Lett.*, *41*, 4020–4026, doi:10.1002/2014GL060130.

Zhang, Y., J. M. Wallace, and D. S. Battisti (1997), ENSO-like interdecadal variability: 1900–93, *J. Clim.*, *10*(5), 1004–1020.

Zheng, F., J. P. Li, R. T. Clark, and H. C. Nnamchi (2013), Simulation and projection of the Southern Hemisphere annular mode in CMIP5 models, *J. Clim.*, *26*(24), 9860–9879.